Diagnostic Studies of Polyolefin Separators in High-Power Lithium-Ion Cells

Robert Kostecki[*z], Laura Norin, Xiangyun Song, and Frank McLarnon[*]

Environmental Energy Technologies Division

Lawrence Berkeley National Laboratory

Berkeley, CA 94720

Abstract

The decrease of ionic conductivity of polymeric separators in high-power Li-ion cells, which were cycled or stored at elevated temperatures, was accompanied by dramatic changes in separator surface morphology. The source and nature of polymer separator degradation in high-power Li-ion batteries have been studied. We attributed the observed porosity loss to a deposit, which precipitated onto the separator surface from the electrolyte and clogged separator pores. This deposit resulted from a homogenous decomposition process of the $LiPF_6$-EC-EMC electrolyte, which was significantly accelerated at elevated temperatures. The electrolyte decomposition products consisted of lithium halophosphates and displayed very strong fluorescence. They contributed to the SEI layers on both cathode and anode where they underwent further oxidation or reduction reactions, respectively.

Key words: Li-ion battery, separator, morphology change, fluorescence, electrolyte decomposition.

[*] Electrochemical Society Active Member

[z] r_kostecki@lbl.gov

Introduction

The battery separator plays an important role by regulating cell kinetics, allowing ionic flow, preventing electronic contact between the two electrodes, and sometimes by acting as a safety device. Because the separator is pressed between the two electrodes and filled with electrolyte, it is in contact with all of the active cell components. By regulating electrolyte distribution, it limits ionic diffusion and recombination rates, and thereby significantly impacts cell capacity, cell power, and available energy. Consequently, much work has been carried out to determine optimal separator characteristics, such as porosity and tortuosity [1-3]. Separator degradation has been often observed in certain types of batteries, and shown to be responsible for battery failure or power loss. Examples of work in this field refer to separator studies in valve-regulated lead acid (VRLA) [4-9], bipolar lead acid [10], nickel/metal hydride [11-13], iron-chromium [14-15], nickel-cadmium [16], and silver-zinc [17] cells. The primary causes of separator degradation are usually attack by electrolyte, dendrite growth through separator pores, structural degradation caused by high temperature or cycling, and the clogging of separator passageways during cycling.

In one instance, low separator electrolyte saturation in consumer VRLA electric vehicle batteries led to escalating oxygen recombination rates that prevented the anode from reaching full charge, causing temperature increase and electrolyte dry-out. This resulted in battery failure after less than four months of use [18]. Resin-bonded paper separators used in lead-acid automotive batteries tend to lose crystallinity when cycled, and salt crystals to accumulate in their pores. The salt deposits reduced the size of the separator pores and eventually bridged pores together, leading to cell shorts. [19]

The reliability of the separator is thus critical for the proper and continued functioning of the cell. There is little reported work on the polyolefin separators used in lithium-ion cells, and their reliability during long-term testing has not been investigated in detail *via* detailed diagnostic

characterization. Our earlier results showed that changes in the separator occur in high-power lithium-ion cells stored at elevated temperatures, and that these changes increase the separator ionic impedance and contribute to the cell power loss [20]. We ascribed that effect to swelling of separator fibers that partially block the pores through which ions traverse, thereby reducing the separator ionic conductivity. Here we report the new results on the origin of this phenomenon and its possible implications on cell performance.

Experimental

The high-power Li-ion cells, which consist of a $LiNi_{0.8}Co_{0.15}Al_{0.05}O_2$ cathode, a synthetic graphite anode, 1.2 M $LiPF_6$ + ethylene carbonate + ethyl-methyl carbonate (EC/EMC) electrolyte, and a Celgard® 2300 tri-layer separator, were manufactured, aged, cycled, and/or abused and then characterized under the U.S. Department of Energy's Advanced Technology Development (ATD) Program [21-22]. In this study we carried out a comparative study of separators removed from control cells that underwent only formation cycles at room temperature (control separator) with separators of cells that were aged at 55°C for up to 40 weeks, losing up to 36% of their initial power (aged separators).

All separators were soaked in dimethyl carbonate (DMC) for 30 minutes after removal from Li-ion cells inside an argon-filled glove box. This eliminated all electrolyte salt from the separator (as verified with infrared spectroscopy) to prevent its reaction with air and moisture. Once in open air, all samples were also rinsed in EMC prior to all analysis in order to remove dust or other contaminants.

Impedance spectra of separators soaked in the electrolyte were recorded inside an argon-filled glove box using a Solartron SI 1260 Impedance Phase Analyzer and a Solartron SI 1286 Electrochemical Interface. The impedance cell and experimental routine were described in ref. [20].

Scanning electron microscope (SEM) images were recorded using a Jeol field emission microscope, model JSM 634OF. Separator samples were coated with gold-palladium before being transferred to the SEM vacuum chamber. Energy dispersive X-ray (EDAX) analysis was carried out using an EDAX attachment to an ISI DS130C dual-stage SEM. Atomic force microscopy (AFM) images were produced in contact mode inside a He-filled glove box, using a Picoscan Molecular Imaging scanning probe microscope coupled with a ThermoMicroscopes Inc. AFM electronic controller.

Thermogravimetric Analysis (TGA) and differential thermal analysis (DTA) of separator samples were recorded under nitrogen between room temperature and 200ºC at a scan rate of 5ºC/min.using a SDT 2960 model by TA Instruments Inc. Fluorescence images of the separators were obtained in the 350-580 nm spectral range using a Nikon Eclipse TE300 microscope, Hamamatsu Orca II camera, model # C4742-98 with a 4x Pan-Fluor objective. Fluorescence spectra of the separators were recorded using a Spex 1404 dual-grating spectrometer and a 325 nm UV laser at 2 mW/cm^2.

Results

AFM images of separators taken from cells aged up to 28 weeks revealed a continuous change of the separator surface structure from a uniform configuration of perpendicular fibers delineating pores to a near-continuous plane of swollen fibers marred by crevices and deep imprints of electrode particles [20]. Figure 1 shows AFM images of a separator extracted from a fresh cell and a cell, which was held at 55^{o}C for 40 weeks. The polypropylene fibers of the aged separator appear to be covered by tightly packed particles of size ~10-200 nm. We believe that the increased fiber thickness and their swollen appearance, which we observed in separators aged for shorter periods of time, is due to the deposition of a residue from the electrolyte. SEM images of the aged separator (Figure 2) confirm our

AFM data and display substantial changes in the separator morphology. Interestingly, the lower magnification images reveal that the distribution of the deposit in the separator is highly non-uniform and exhibits a patchy pattern. There remain areas which show no or little change compared to the original morphology whereas some regions are completely covered by a thick deposit layer.

The compounds covering the fibers significantly reduce both the size of the pores and the homogeneity of the separator, thereby increasing the mean path length of the ions, and consequently increasing the potential drop across the separator. To evaluate this effect and its possible consequences on the separator performance, the average ionic conductivity of the separators was determined by impedance spectroscopy. The impedance spectra of separator samples, which were soaked in the electrolyte and pressed between two Ni electrodes, are shown in Figure 3. The high-frequency end of the impedance spectrum, which corresponds to the separator ionic resistance, shifts continuously toward higher resistances with increasing cell storage time. The loss of porosity and uniformity that was observed with TEM and ATM could be directly responsible for the impedance increase by reducing the amount of electrolyte trapped within the separator and/or decreasing the size of pores and channels. Both effects can lead to significant impediment of Li-ions transport.

First insight into the nature of the deposit was obtained with TGA/DTA characterization (Fig. 4). A thermo-gravimetric curve of a fresh separator shows no visible changes as it is heated up to 120ºC. However, a separator sample taken from a cell aged for 40 weeks at 55^{o}C undergoes a 1% mass loss at 47ºC and then a continuous slower loss out to 120ºC. This mass loss is accompanied by a slight baseline shift in the DTA, indicating an endothermic nature of the process associated with the observed changes on the TGA curve. The rapid decrease of mass at T<50^{o}C is most likely due to evaporation of organic solvents, which may still have been trapped inside the pores. However, the steady decrease of sample mass observed at higher temperatures is related to the deposit decomposition process.

Further evidence of the nature and origin of the deposit was obtained from EDAX analysis of the aged separators. The EDAX spectrum (Figure 5) of a separator extracted from a cell that was held at 55^{o}C for 40 weeks shows a very strong signal, which arises from phosphorous compounds. The silicon peak at 1.72 keV originates from the sample holder that was used in this experiment. The phosphorous peak is not present in the spectrum of a separator that was removed from a fresh cell, which not only indicates that the salt ($LiPF_6$) is not the source of P-signal in the EDAX spectrum, but also confirms that the salt was completely removed during rinsing in DMC. Thus, the phosphorous derives from the electrolyte decomposition products, which precipitate uniformly on the separator and the electrodes.

All attempts to identify the composition of the deposit by Raman spectroscopy were hampered by very strong fluorescence from the aged separators. The Raman peaks that arise from polypropylene and polyethylene, which are easily identifiable on the spectra of a fresh separator (not shown here), were completely obscured by the fluorescence signal. The polyolefin peaks could not be detected even after soaking the separator samples in DMC for a full week. Soaking them in water for several days somewhat reduced the intensity of the fluorescence but not to the extent necessary to detect Raman signals arising from the separator and the deposit. Interestingly, local heating from the laser beam could remove the fluorescence signal and restore the original separator peaks, but as a consequence of the heating no signal from the deposit could be seen. The observed thermal instability of the deposit is consistent with our TGA results.

We used fluorescence microscopy to investigate these phenomena further and found that aged separators emit fluorescence across a broad range of excitation (350-580 nm) and emission (350-660 nm) wavelengths. A typical fluorescence image of a separator removed from an aged Li-ion cell displays a non-uniform patchy pattern of spots which are fluorescent and areas which show no emission at all (Fig. 6). Interestingly, parts of the Li-ion cell separator that extended beyond the edges

of the electrodes in the cell show uniform and strong fluorescence that apparently originates from a film that is spread evenly atop or throughout the separator. Fluorescence imaging of the cathode and anode harvested from the aged cell reveal that their surface exhibit areas of fluorescence activity; however, the emission intensity was significantly smaller than for the separator.

Fluorescence spectroscopy of separator samples, shown in Figure 7, uncovers a difference in intensity and composition between the deposits on the separator that had not been in contact with the electrodes in the cell and the separator that had been sandwiched between the electrodes. The no-electrode separator shows very strong fluorescence with three bands at 375, 388, and 402 nm and a featureless broad maximum centered at ca. 470 nm. Interestingly, parts of the separator that were in contact with electrodes show completely different spectral characteristic. The intensity of the fluorescence emission drops by half, which is probably due to the non-uniform fluorescence pattern observed by the microscope. The sharp bands at ~ 390 nm disappear, and the broad maximum shifts to 550 and 600 nm for the cathode and anode sides of the separator, respectively. Interestingly, the fluorescence signal on the anode side was always slightly stronger than on the cathode side.

Discussion

Interaction between the electrolyte or electrolyte decomposition products and the electrodes is well established. Electrolyte decomposition on the anode is a known phenomenon that is responsible for the SEI formation on the anode surface. More recently, SEI layer formation on the $LiMn_2O_4$ cathode has also been reported [23]. Kanamura et al. implicate $LiCoO_2$ cathodes as having catalytic effects on propylene carbonate (PC) electrolyte. PC is oxidized on the $LiCoO_2$ surface through chemical reactions with oxidation products of anions and/or electrolyte impurities, and the reaction products are adsorbed on the cathode surface. [24] A similar phenomenon was observed with $LiNiO_2$

cathodes in $LiPF_6$-EC-EMC. [25] Additionally, Jang [26] and Baba [27] found that decomposition products of $LiPF_6$ interact with $LiMn_2O_4$ and $LiCoO_2$ cathodes, respectively, and cause the dissolution of cathode active material in $LiMn_2O_4$ spinel. Zaban and Aurbach reported that a primary product of electrode/$LiPF_6$-containing electrolyte interaction is a $Li_xPO_yF_z$ compound [28]. Ostrovskii et al. confirmed the presence of phosphorous compounds in the cathode SEI layer [29]. Balasubramanian et al. reported the presence of LiF at the surface of cycled $LiNi_{0.85}Co_{0.15}O_2$ cathodes, and reported that the LiF arose from the decomposition of $LiPF_6$ salt [30]. Sloop at al. reported on such a decomposition at elevated temperatures [31,32]. They postulated that $LIPF_6$ acts as a Lewis acid with EC-containing solvents to generate transesterification products, PEO polymers, and CO_2. Ravdel at al. investigated thermal decomposition of $LIPF_6$ in organic carbonates, and they detected $ROPF_4$, $(RO)_2PF_3$, $(RO)_3PF_3$, OPF_3, $OPF_2(OR)$, and $OPF(OR)_2$ among the electrolyte decomposition products [33]. However, none of the proposed decomposition products of $LIPF_6$ in organic carbonates is expected to generate a fluorescence signal.

We postulate that the deposit observed on the cell separator originates from the $LiPF_6$, EC:EMC electrolyte thermal decomposition. The phosphorous-containing products precipitate on the separator and the electrodes during storage at elevated temperatures. Our studies of these products at various locations on the separator and electrodes indicate that they result from a two-stage electrolyte decomposition process: homogenous decomposition followed by heterogeneous redox reactions at specific areas, that are in contact with the electrodes.

Homogenous electrolyte decomposition proceeds everywhere in the cell, and its inorganic products are characterized by a broad and intense fluorescence. The shape of the fluorescence spectra, their peak positions as a function of wavelength, and the strength of the transition involved in fluorescence are spectroscopic characteristics that are sensitive to molecular conformation and

symmetry. Because fluorescence in organic compounds arises from delocalized electrons in conjugated double bonds [34], in the fluorescence we observe most likely originates from an inorganic crystalline solid. Inorganic fluorescence is usually associated with metal ions embedded in a relatively inert matrix such as a metallic oxide, phosphate, silicate, etc. The featureless character of the fluorescence spectra of the separator suggest that the deposits we observe consists of halophosphates, likely an $LiPO_x$:LiF compound, with lithium fluoride as an activator. Halophosphates fluoresce when co-crystallized with such an impurity, giving rise to a broad emission spectrum (400-700 nm) akin to what was observed from the separator [35].

This electrode-specific redox reactions account for the fluorescence asymmetry observed on the Li-ion cell separators and their phosphorous-containing products, which were detected on the anode and cathode by EDAX and Raman microscopy. It is known that oxidation or reduction of fluorescent materials often results in quenching of the fluorescence [36]. This phenomenon likely accounts for the conversion of the halophophates into non-fluorescent pyrophosphate- and methaphospate-type compounds on the cathode and anode side of the separator, respectively. Thus, the origin of the phosphorous compounds in the SEI layers in both the cathode and the anode is most likely a result of the $LiPF_6$ EC:EMC electrolyte homogeneous decomposition and the subsequent electrochemical reactions of the precipitate at the electrodes rather than direct redox decomposition of $LiPF_6$ on either electrode.

The electrolyte decomposition products form a thick film on the separator, which partially clogs the pores and thereby impedes lithium-ion transfer. It is responsible for the increase of the cell impedance and accounts for about 10% of the total cell impedance increase [20]. More importantly, the electrolyte decomposition products contribute to the electrode SEI layers and tend to accumulate with time, contributing to the impedance rise on both electrodes.

Conclusions

The central position of the separator within the cell makes it a useful tool with which to study cell degradation processes. Processes that occur in the electrolyte or at either electrode/electrolyte interface may be imprinted or otherwise reflected in the characteristics of the separator surfaces. We have confirmed our earlier observations of the separator morphology changes upon storage in a cell containing $LiPF_6$, EC:EMC electrolyte at elevated temperatures. These changes are caused by non-uniform distribution of deposits that partially cover the separator surface and clog the pores increasing its local ionic impedance. These deposits originate from the electrolyte homogenous decomposition process and consist of halophosphates $LiPO_x$:LiF, which are responsible for the observed strong fluorescence emission. They further undergo a series of subsequent reduction and oxidation processes at the anode and cathode surfaces, leading to formation of metaphosphates and pyrophosphates, respectively. Their contribution to the SEI layers on both electrodes is likely to affect the impedance of the Li-ion intercalation/deintercalation processes and thereby influence the electrochemical performance of the cell.

Acknowledgments

This work was supported by the Assistant Secretary for Energy Efficiency and Renewable Energy, Office of FreedomCAR and Vehicle Technologies of the U.S. Department of Energy under Contract No. DE-AC03-76SF00098. The authors gratefully acknowledge the help of Michael Baksh of U.C. Berkeley with the fluorescence microscopy and the help of Henning Feick of Lawrence Berkeley National Laboratory with the fluorescence spectroscopy, as well as the tested cells, help, and advice provided by the ATD Program participants.

References

1. F. G. B. Ooms, E. M. Kelder, J. Schoonman, N. Gerrits, J. Smedinga and G. Calis, *J. Power Sources*, **97**, 598 (2001).
2. A. Magistris, P. Mustarelli, F. Parazzoli, E. Quartarone, P. Piaggio and A. Bottino, *J. Power Sources*, **97**, 657 (2001).
3. G. Venugopal, J. Moore, J. Howard and S. Pendalwar, *J. Power Sources*, **77**, 34 (1999).
4. W. Bohnstedt, *J. Power Sources*, **95**, 234 (2001).
5. T.G. Chang, D. M. Jochim, *J. Power Sources*, **91**, 177 (2000).
6. D. Pavlov, S. Ruevski, V. Naidenov, G. Sheytanov, *J. Power Sources*, **85**, 164 (2000).
7. D. Pavlov, S. Ruevski, V. Naidenov, *Proc. of the Sixteenth Annual Battery Conf. on Applications and Advances*, 169 (2001).
8. B. Culpin, D.A.J. Rand, *J. Power Sources*, **36**, 415 (1991).
9. R.J. Ball, R. Kurian, R. Evans, R. Stevens, *J. Power Sources*, **104**, 234 (2002).
10. M. Coux, X. Muneret, P. Lenain, J.L. Wojkiewicz, J. Renard, *J. Power Sources*, **78**, 115 (1999).
11. S. Cheng, J. Zhang, H. Liu , Y. Leng , A. Yuan and C. Cao *J. Power Sources*, **74**, 155 (1998).
12. M. Ikoma, Y. Hoshina, I. Matsumoto, C. Iwakura, *J. Eletrochem. Soc.,* **143**, 1904 (1996).
13. J. Bennett, W.M. Choi, *Proc. of the Thirteenth Annual Battery Conf. on Applications and Advances*, 153 (1998).
14. R.A. Assink, *J. Separator Science*, **17**, 205 (1984).
15. L.W. Hruska, R.F. Savinell, *J. Electrochem. Soc.,***128**, 18 (1981)..
16. S. Gross, *Energy Conversion*,.**11**, 39 (1971).
17. T. Danko, *Proc. Eleventh Annual Battery Conf. on Applications and Advances*, 283 (1996).
18. R.D. Brost, R.D. *Fifteenth Annual Battery Conf. on Applications and Advances*, 243 (1999).

19. J.R. Dafler, F.W. Wentzel, Jr., B. Campbell, D.L.K. Chu, *J. Electrochem. Soc.,* **123**, 780 (1976).

20. L. Norin, R. Kostecki, R. McLarnon, *Electrochem. and Solid State Letters*, **5**, A67 (2002).

21. 2001 Annual Progress Report for the Advanced Technology Development Program, U.S. Department of Energy, Feb. 2002, http://www.cartech.doe.gov/pdfs/B/196.pdf

22. X. Zhang, P. N. Ross, Jr., R. Kostecki, F. Kong, S. Sloop, J. B. Kerr, K. Striebel, E. J. Cairns and F. McLarnon, *J. Electrochem. Soc*., 148 (2001) 463.

23. Y. Matsuo, R. Kostecki, F. McLarnon,, *J. Electrochem. Soc.,* **148**, (2001) A687.

24. K. Kanamura, T. Umegaki, M. Ohashi, S. Toriyama, S. Shiraishi, Z. Takehara, *Electrochimica Acta*, **47,** 433 (2001).

25. D. Aurbach, K. Gamolsky, B. Markovsky, G. Salitra, Y. Gofer, U. Heider, R. Oesten, M. Schmidt, *J. Electrochem. Soc.* **147**, 1322 (2000).

26. D. H. Jang, Y. J. Shin, and S. M. Oh, *J. Electrochem. Soc*., **143,** 2204 (1996).

27. Y. Baba, S. Okada and J. Yamaki, *Solid State Ionics*, **148**, 311(2002).

28. Zaban, D. Aurbach, *J. Power Sources*, **54,** 289, (1995).

29. D. Ostrovskii, F. Ronci, B. Scrosati, P. Jacobsson, *J. Power Sources*, **94**, 183 (2001)

30. M. Balasubramanian, H.S. Lee, X. Sun, X.Q. Yang, A.R. Moodenbaugh, J. McBreen, D.A. Fischer, Z. Fu, *Electrochem. and Solid State Letters*, **5**, A22 (2002).

31. S.E. Sloop, J.K. Pugh, S. Wang, J.B. Kerr, K. Kinoshita, *Electrochem. and Solid State Letters*, **4**, A42 (2001).

32. S.E. Sloop, J.B. Kerr, K. Kinoshita*, J. Power Sources*, **119-121**, 330 (2003)

33. B. Ravdel, K.M. Abraham, R. Gitzendanner, J. DiCarlo, B. Lucht, C. Campion, *, J. Power Sources*, **119-121**, 805 (2003)

34. J. Lakowicz, *Principles of Fluorescence Spectroscopy*, Plenum Press, NY, **1** (1983).

35. P. Johnson in *Luminescence of Inorganic Solids,* P. Goldberg, editor, pp 287-292, 305, Academic Press, NY (1966)

36. P. Pringsheim and M. Vogel, *Luminescence of Liquids and Solids*, Interscience Publishers, Inc., NY, 33 (1943).

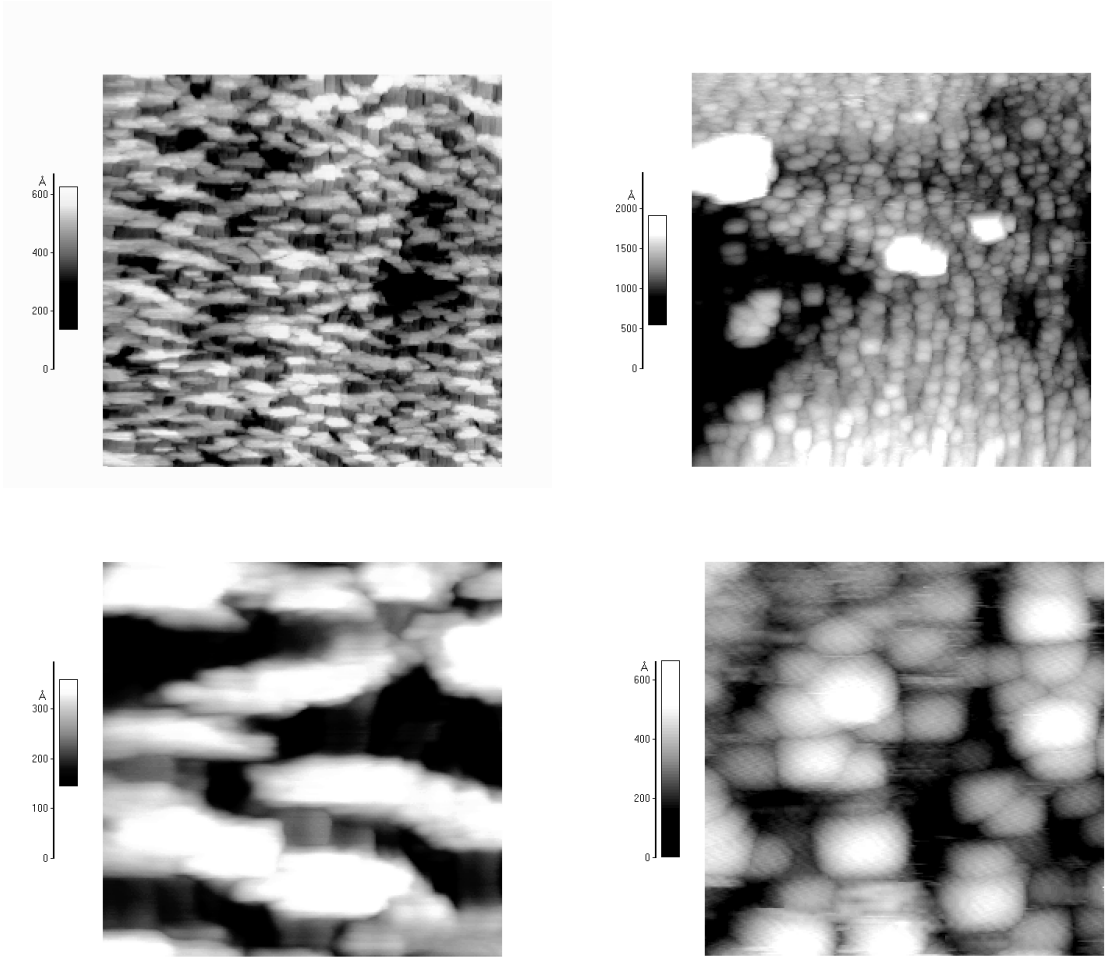

Figure 1. AFM images of separators extracted from (a) fresh cell, (b) cell stored at 55°C for 40 weeks.

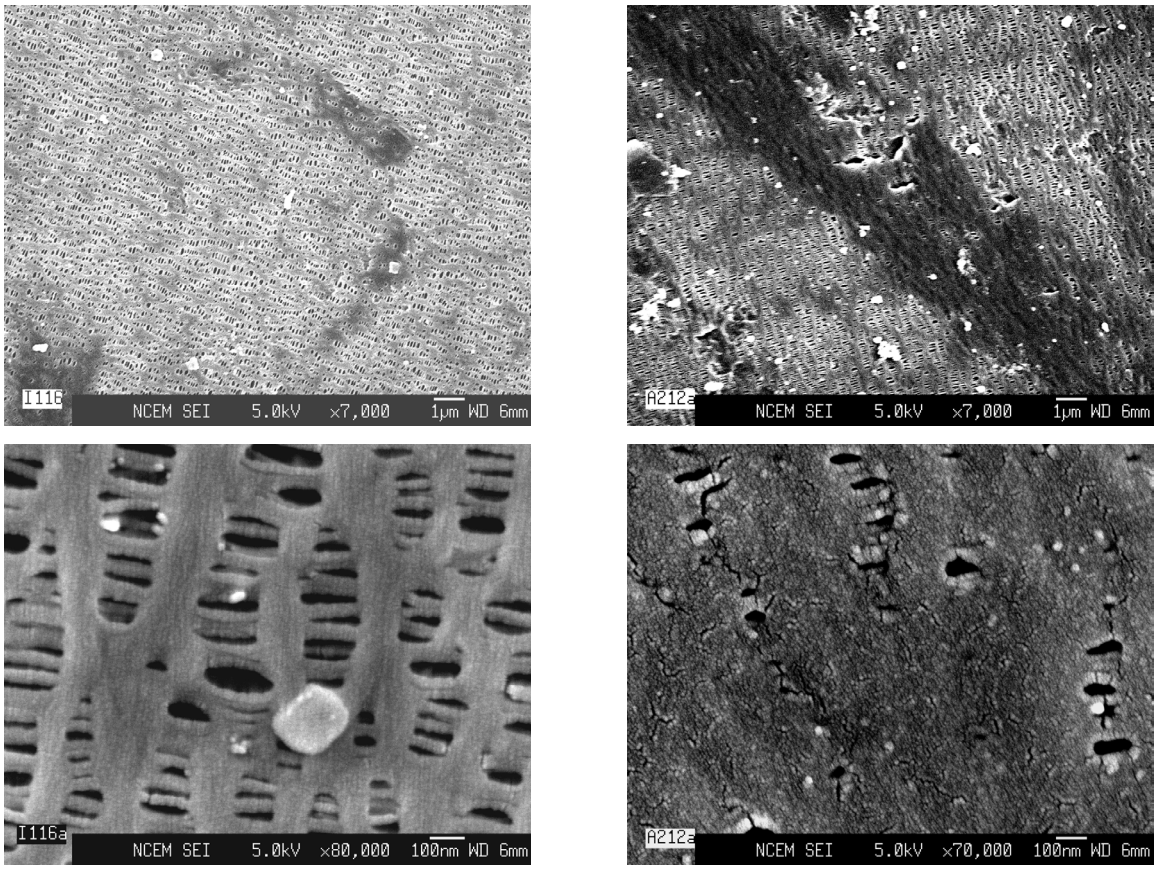

Figure 2. SEM images of separators extracted from (a) fresh cell, (b) cell stored at 55°C for 40 weeks.

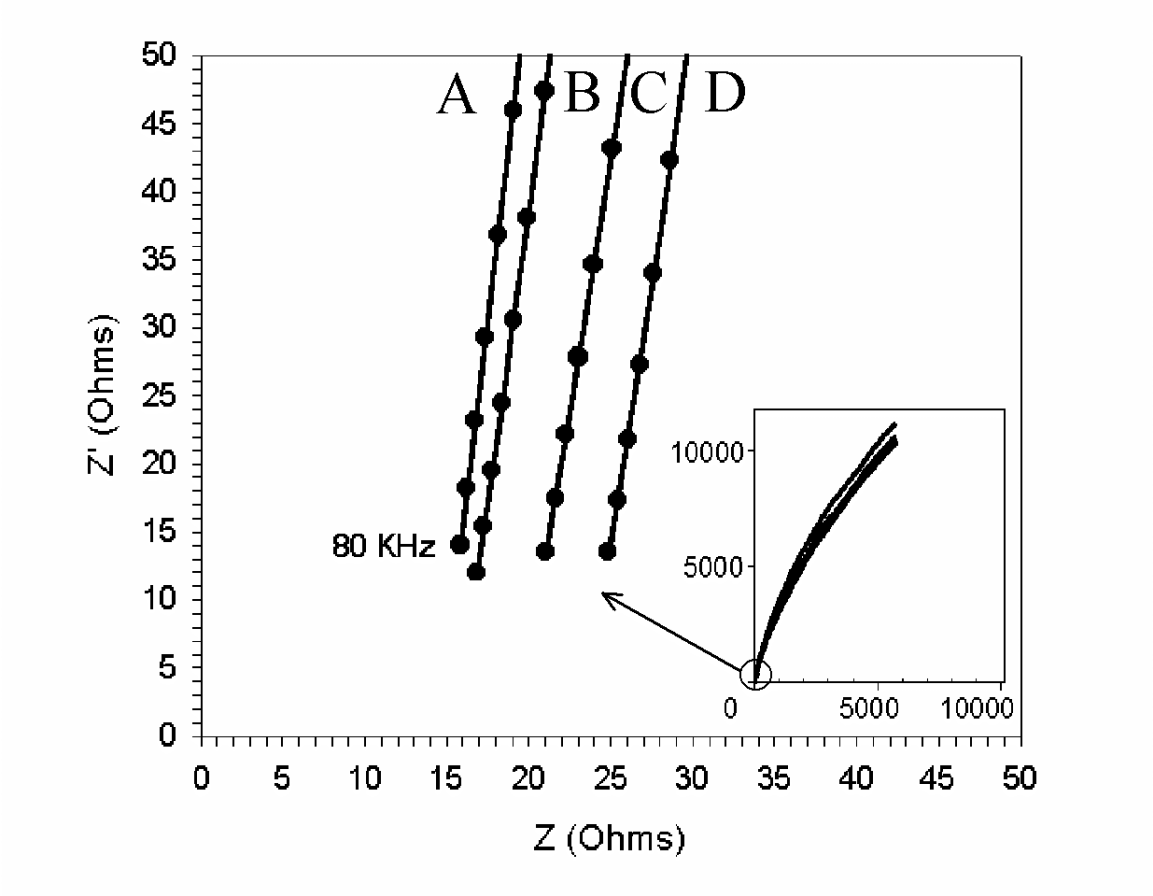

Figure 3. Impedance spectra of separators removed from (a) fresh cell, and cells stored at 55°C for (b) 8 weeks, (c) 24 weeks, and (d) 40 weeks.

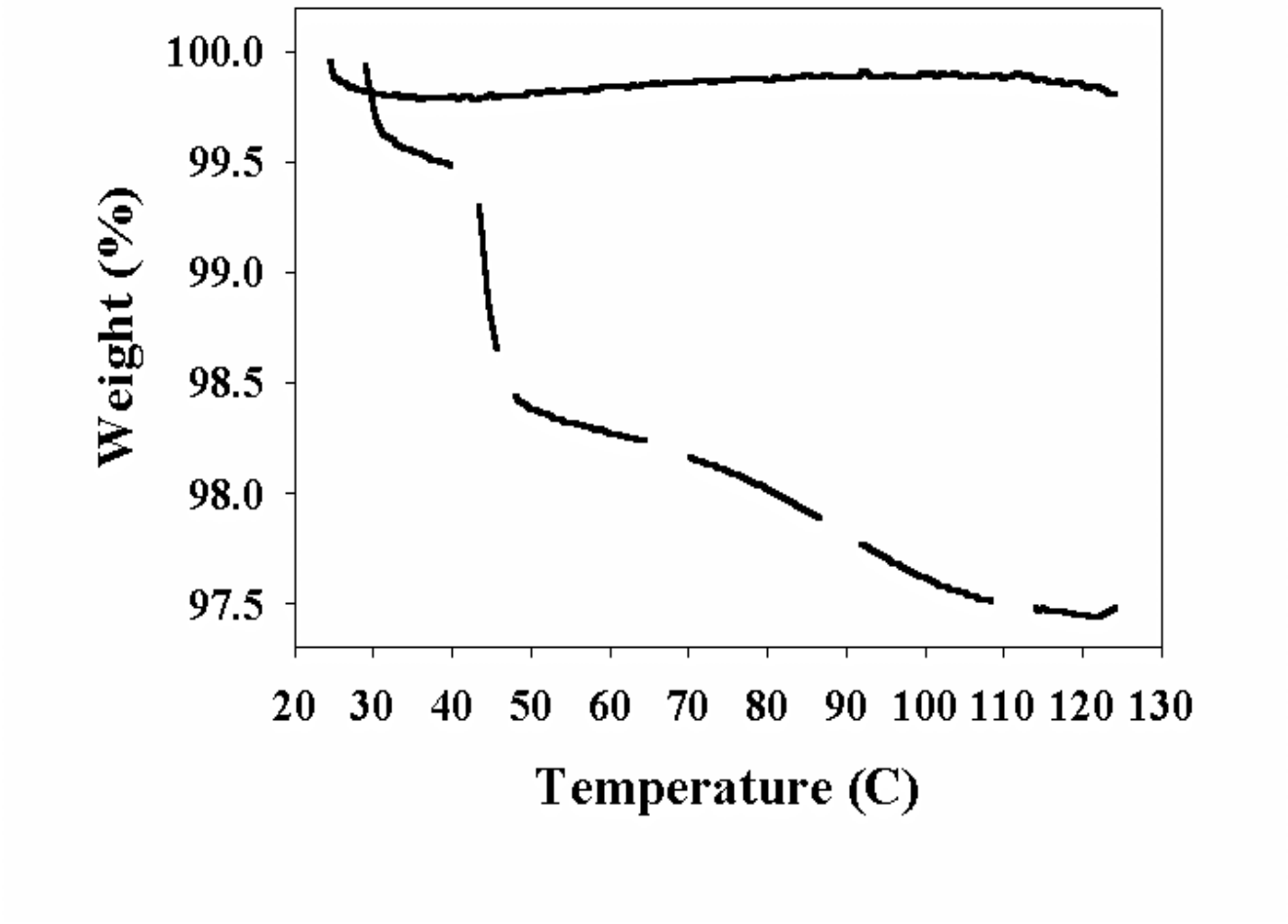

Figure 4. TGA curves of fresh Celgard 2300 (solid line) and separator removed from the cell stored at 55°C for 40 weeks (dashed line).

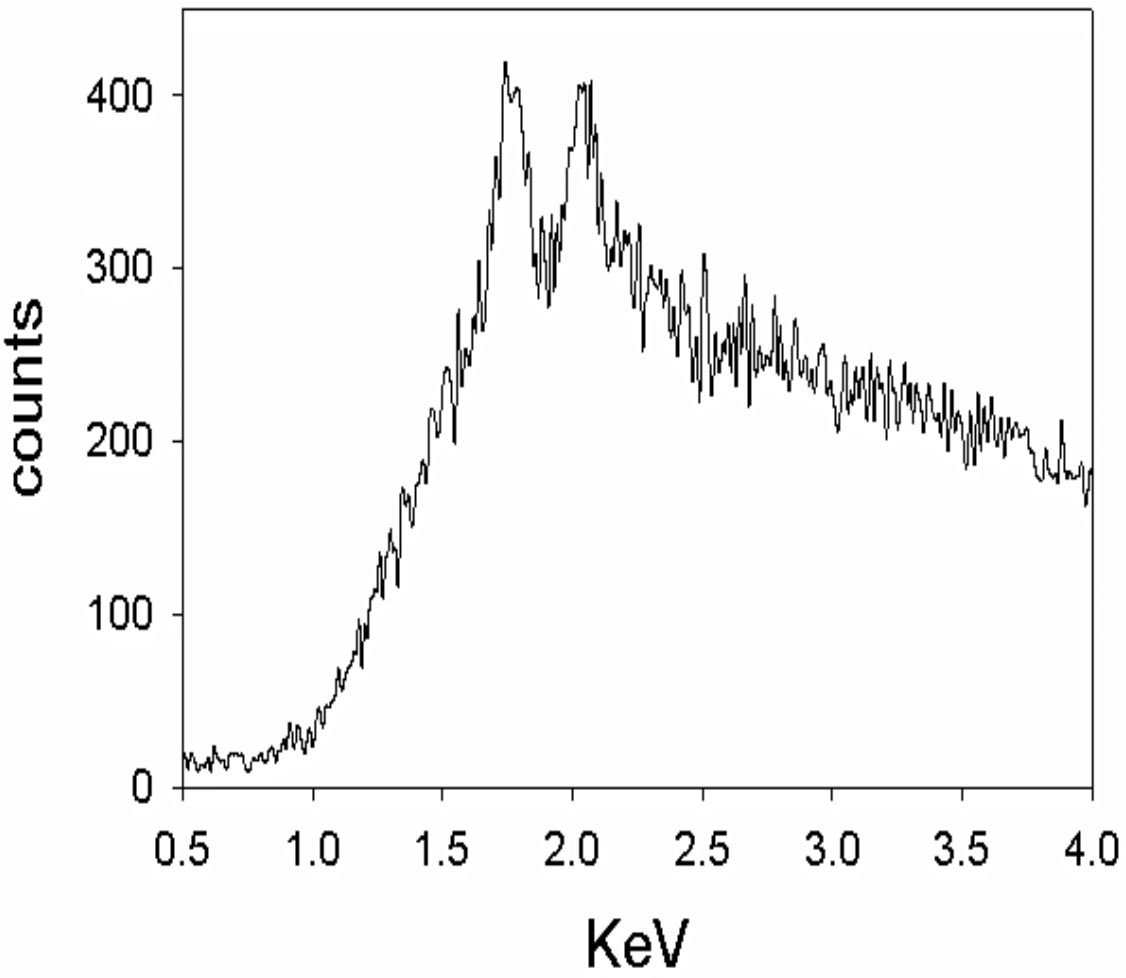

Figure 5. EDAX spectra of an aged separator. The silicon peak at 1.72 KeV originated from the sample holder.

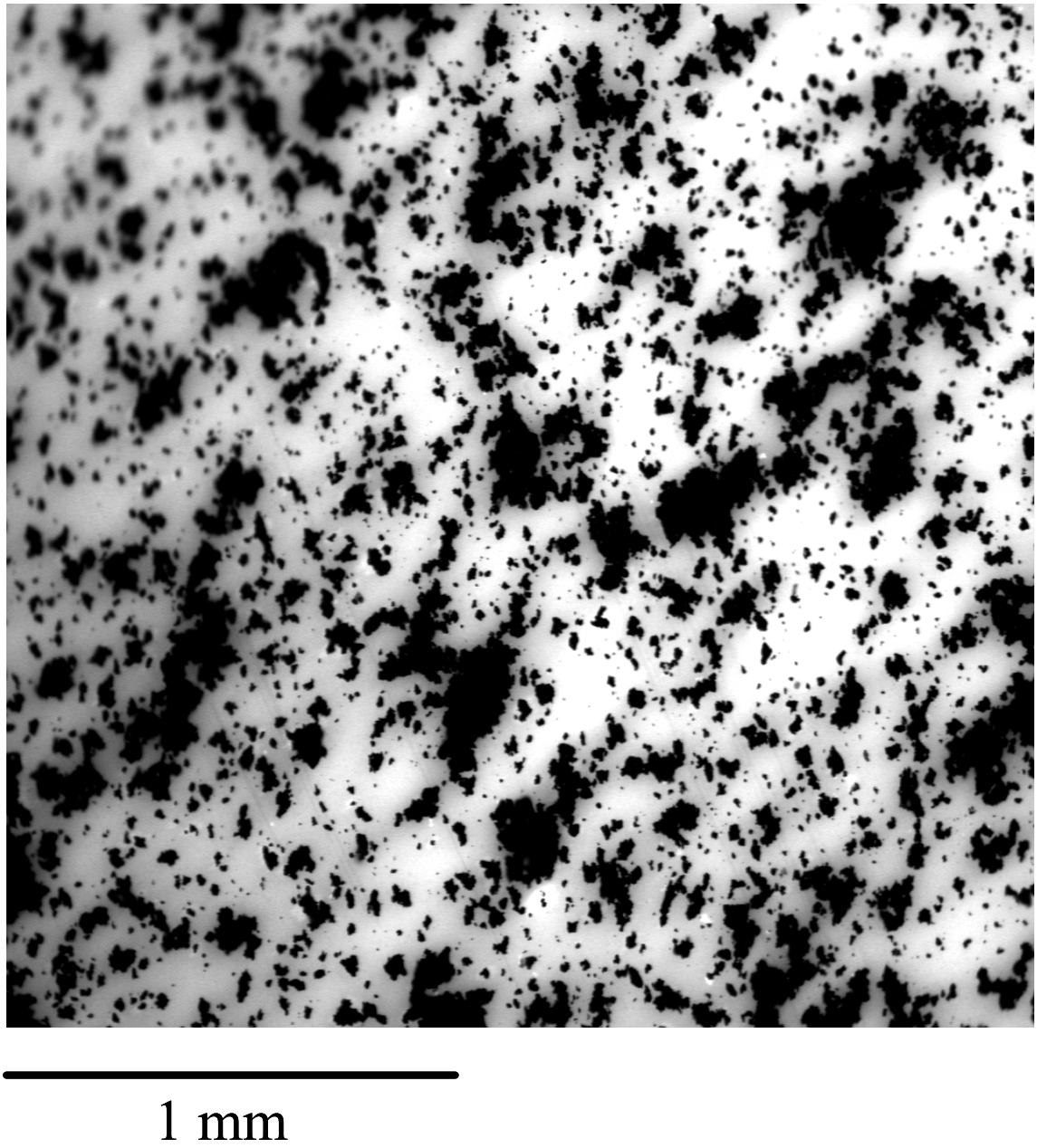

Figure 6. 2.5x2.5 mm fluorescence image obtained in the 350-580 nm spectral range of a separator aged in a cell for 40 weeks at 55ºC. Bright areas correspond to intense fluorescence emission, dark patches are non-fluorescent.

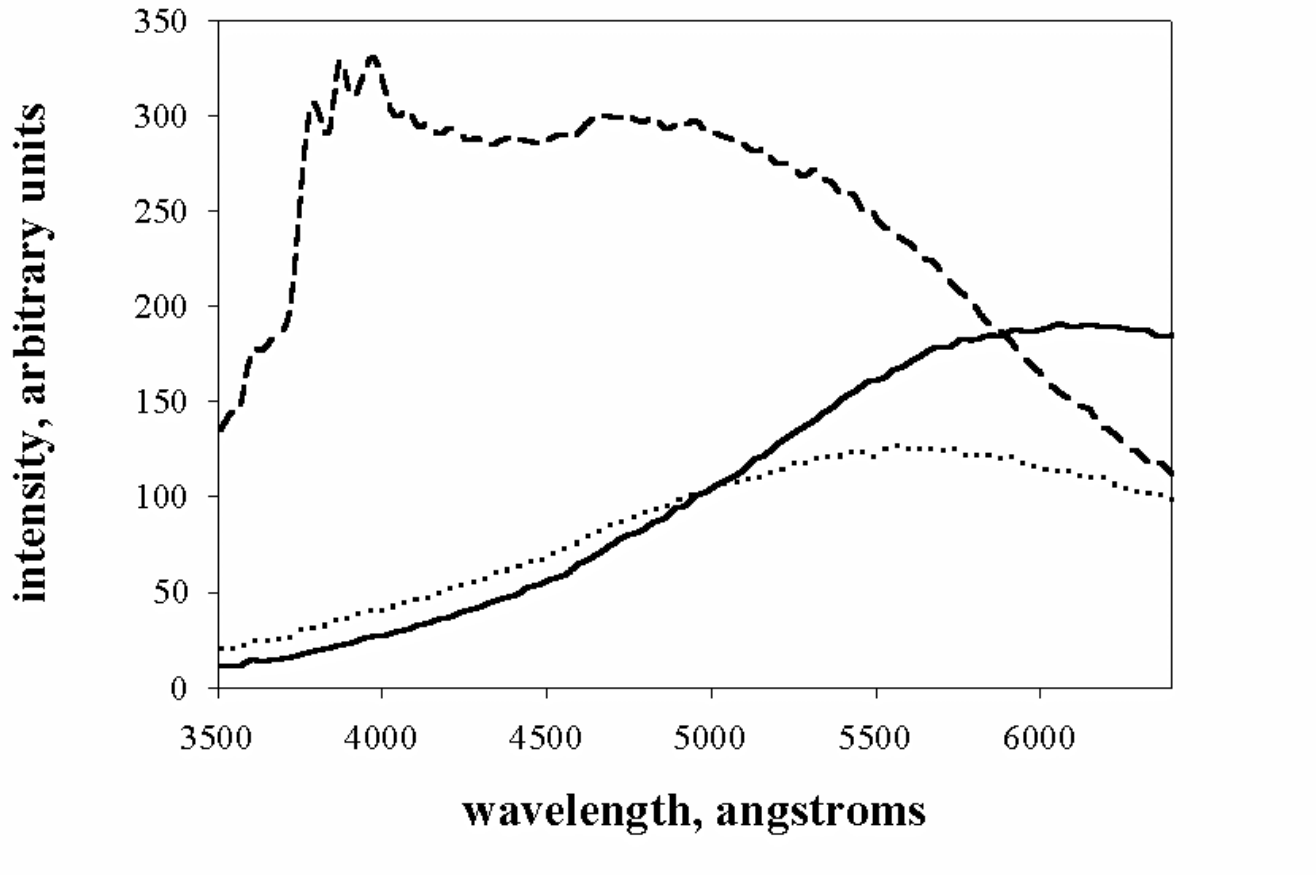

Figure 7. Fluorescence spectra of three parts of the separator: two sections that were in contact with the anode or cathode inside the cell and a section that was not in contact with the electrodes. Excitation light source: 325 nm UV laser at 2 mW/cm^2.